Chapter 7
Genetically Encoded Fluorescent Probes for Intracellular Zn^{2+} Imaging

Anne M. Hessels and Maarten Merkx

Abstract In this chapter we provide an overview of the various genetically encoded fluorescent Zn^{2+} sensors that have been developed over the past 5 to 10 years. We focus on sensors based on Förster resonance energy transfer (FRET), as these have so far proven to be the most useful for detecting Zn^{2+} in biological samples. Our goal is to provide a balanced discussion of the pros and cons of the various sensors and their application in intracellular imaging. Following the description of the various sensors, several recent applications of these sensors are discussed. We end the chapter by identifying remaining challenges in this field and discussing future perspectives.

Keywords Fluorescence • FRET • Imaging • Microscopy • Sensor • Zinc

7.1 Introduction

Transition metals such as zinc pose an interesting dilemma for living organisms because they are essential cofactors for numerous enzymes and proteins, but at the same time are toxic even at low concentrations in their free form (Valko et al. 2005). Mechanisms to control this delicate balance may vary for different metal ions and also between organisms. Copper homeostasis in eukaryotes has been shown to involve specific copper chaperone proteins that transfer Cu^{+} to various cellular targets without releasing it into the cytosol (Rae et al. 1999). Similar chaperones have not been identified for Zn^{2+}; instead, a general Zn^{2+}-buffering mechanism has been proposed in which the free cytosolic Zn^{2+} concentration in mammalian cells is kept constant at pM–nM levels (Cousins et al. 2006; Krezel and Maret 2006). The free concentration of Zn^{2+} is also likely to differ substantially between subcellular locations, as mM concentrations of total Zn^{2+} have been reported for pancreatic β-cell granules (Hutton et al. 1983) and inferred for secretory vesicles in neuronal (Linkous et al. 2008) and mast cells (Ho et al. 2004).

A.M. Hessels • M. Merkx (✉)
Laboratory of Chemical Biology and Institute of Complex Molecular Systems, Department of Biomedical Engineering, Eindhoven University of Technology, Eindhoven, The Netherlands
e-mail: m.merkx@tue.nl

© Springer Japan 2014

T. Fukada, T. Kambe (eds.), *Zinc Signals in Cellular Functions and Disorders*,
DOI 10.1007/978-4-431-55114-0_7

To advance our understanding of zinc homeostasis and the putative role of Zn^{2+} in (intracellular) signal transduction, tools are required that allow direct (sub) cellular imaging of Zn^{2+} concentrations in single living cells in real time. Fluorescence is ideally suited for this purpose, because it combines high sensitivity with subcellular resolution (Kikuchi 2010). Such fluorescent sensors should have an appropriate affinity for Zn^{2+} under physiological conditions, show high selectivity for Zn^{2+} over other biologically abundant metals, and translate Zn^{2+} binding into a strong increase in fluorescence, or even better, a ratiometric change in fluorescent properties. Currently, Zn^{2+}-sensitive fluorescent dyes are still the most commonly imaging probes for monitoring Zn^{2+} in biological samples. The development of synthetic sensors continues to be an active area in chemical biology, and an impressive variety of Zn^{2+}-sensitive fluorescent dyes (such as Zinquin, rhodzin-3, and FluoZin-3) has been developed, some of which have also been applied to monitor Zn^{2+} fluctuations in living cells (Domaille et al. 2008; Nolan and Lippard 2009). However, synthetic probes come with some intrinsic limitations, notably a lack of full control over subcellular localization and the need to achieve high intracellular concentrations of the dye, which may perturb free levels of Zn^{2+}. In addition, it has proven challenging to create synthetic dyes that rival the affinity and specificity typically observed with metalloproteins, which is important to reliably determine the extremely low concentrations of Zn^{2+} and other transition metal ions (Krezel and Maret 2006; Bozym et al. 2006; Van Dongen et al. 2007).

Genetically encoded fluorescent sensors offer several advantages compared to small molecule-based probes. Small-molecule probes need to enter the cell via diffusion over the cell membrane. Although these probes can be trapped by hydrolysis of methylesters by intracellular esterases, controlling their concentration over prolonged time intervals remains challenging. Even more importantly, once inside the cell, little control over subcellular localization is possible, which is an important caveat given that Zn^{2+} concentrations can vary considerably between different organelles. Protein-based, genetically encoded probes are produced by the cell itself, which in principle allows control over their intracellular concentration, prevents leakage, and provides excellent control over intracellular localization. A second advantage of genetically encoded probes is that they allow one to take advantage of the excellent affinity and specificity displayed by natural metal-binding proteins, which can be further improved by both rational and directed evolution approaches. Although adding a fluorescent dye to a cell maybe slightly easier than relying on DNA transfection, the choice of useful commercially available Zn^{2+} dyes is limited, which presents an important restriction for those scientists who cannot synthesize these probes themselves. DNA-encoded probes, on the other hand, can be easily replicated by standard molecular biology techniques and distributed through depositories such as AddGene.

Most applications of genetically encoded fluorescent sensors have been limited to studies in immortalized cell lines using transient transfection, but genetically encoded fluorescent sensors can also be applied in primary cells using viral vectors or even entire organisms. Although at present the latter still requires a substantial effort, new developments in genetic engineering are expected to make the latter

possibility more readily accessible in the future. In this chapter we provide an overview of the various genetically encoded fluorescent Zn^{2+} sensors that have been developed during the past 5 to 10 years. We focus on sensors based on Förster resonance energy transfer (FRET), as these have so far proven to be the most useful for detecting Zn^{2+} in biological samples. Our goal is to provide a discussion of the pros and cons of the various sensors and their application in intracellular imaging. Following the description of the various sensors, several recent applications of these sensors are discussed. We end the chapter by identifying remaining challenges in this field and discussing future perspectives.

7.2 Genetically Encoded Zn^{2+} Sensors

7.2.1 Sensor Principles

Several strategies have been explored to develop Zn^{2+}-responsive fluorescent proteins. One approach is to introduce a Zn^{2+}-binding site close to the chromophore of the fluorescent protein. This principle was first reported by Barondeau et al., who created a Zn^{2+}-binding variant of green fluorescent protein (GFP) in which the tyrosine that is part of the original fluorophore was replaced by a metal-coordinating histidine (Barondeau et al. 2002). This sensor binds both Zn^{2+} and Cu^{2+} with micromolar affinity. A twofold increase in fluorescence intensity was observed upon addition of Zn^{2+}, whereas Cu^{2+} binding resulted in quenching of fluorescence. This sensor has not been used beyond the initial proof of concept study, however, most likely because its affinity for Zn^{2+} is too weak for intracellular Zn^{2+} detection and because it is not easily calibrated. Another strategy for single-domain fluorescent Zn^{2+} sensors was reported by Mizuno et al., who fused de novo designed metal ion-responsive coiled-coil peptides with circularly permutated green fluorescent protein (cpGFP) (Mizuno et al. 2007). Metal binding to histidine residues in these peptides induces a structural change from a random coil structure to an α-helical, trimeric, coiled-coil structure, which stabilizes the cpGFP domain and results in an increase in fluorescence. Although the Zn^{2+} affinity for this probe was higher than the sensor reported by Barondeau ($K_d = 570$ nM), binding of Cu^{2+} and Ni^{2+} resulted in similar increase in fluorescence.

More recently, incorporation of metal-chelating, non-natural amino acids has been explored to obtain metal-responsive fluorescent proteins. Wang and coworkers developed a circularly permuted variant of super folder GFP in which the tyrosine present in the chromophore was replaced by 8-hydroxyquinolin-alanine (HqAla), yielding a fluorescent sensor that showed a sevenfold increase in fluorescent intensity in the presence of Zn^{2+} ($\lambda_{ex} = 495$ nm; $\lambda_{em} = 537$ nm) (Liu et al. 2013b). In contrast to the two other examples just discussed, Zn^{2+} binding also results in a blue shift of both excitation and emission spectra, allowing ratiometric detection. At present the applicability of this probe is still limited, not

only by the requirement to use non-natural amino acids but also because of the relatively weak Zn^{2+} affinity ($K_d = 50–100$ μM). Besides their relatively low Zn^{2+} affinities and metal specificity, most single-domain fluorescent sensor proteins are intensity based, that is, they show an increase or decrease in fluorescence but their spectral properties do not change. This is a disadvantage for quantitative intracellular applications (Liu et al. 2013a), because fluorescence intensity is not only a function of the Zn^{2+} concentration but also depends on expression levels and can be affected by photobleaching.

The most commonly used strategy to design fluorescent sensor proteins takes advantage of the principle of Förster resonance energy transfer (FRET). FRET is a mechanism in which excitation energy is transferred from a donor to an acceptor fluorescent domain. The efficiency of this process is distance- and orientation dependent and therefore useful to detect conformational changes as a result of metal binding to a receptor domain. FRET-based Zn^{2+} sensors consist of one or more metal-binding domains flanked by a donor and acceptor fluorescent domain. The most frequently used FRET pair consists of cyan fluorescent protein (CFP) and yellow fluorescent protein (YFP), although more red-shifted FRET pairs have recently also been reported (Lindenburg et al. 2013; Miranda et al. 2012). A key advantage of FRET-based sensors is that they are ratiometric, that is, the ratio of acceptor and donor emission provides a measure of the metal-binding state that is independent of the sensor concentration. In principle, FRET sensor design is also more modular, although developing FRET sensors with a large change in emission ratio can be challenging and often requires much optimization. Other important properties that determine the performance of FRET-based sensors for intracellular Zn^{2+} imaging are their Zn^{2+} affinity and specificity, their binding kinetics, and their pH sensitivity. In the next paragraph we discuss the various FRET-based Zn^{2+} sensor systems that have been developed thus far and discuss these aspects. The first family of Zn^{2+} sensors that we discuss, the CALWY-sensors, will also be used to introduce some of the general issues that are important when considering the applications of these sensors.

7.2.2 Genetically Encoded FRET-Based Sensors

7.2.2.1 CALWY Sensors

Sensors from the CALWY family consist of two small metal-binding domains, Atox1 and WD4, that each contain a metal-binding CXXC motif, fused by a long and flexible linker. In the original sensor (CALWY), the metal-binding domain was flanked by cyan and yellow fluorescent domains, hence their name (CFP-Atox1-Linker-WD4-YFP) (Fig. 7.1a) (Van Dongen et al. 2006; Van Dongen et al. 2007). ATOX 1 and WD4 are native Cu(I)-binding domains that play a role in maintaining copper homeostasis, and the sensor was initially developed to create a genetically encoded Cu^{+} sensor based on the Cu^{+}-induced dimerization of these two domains.

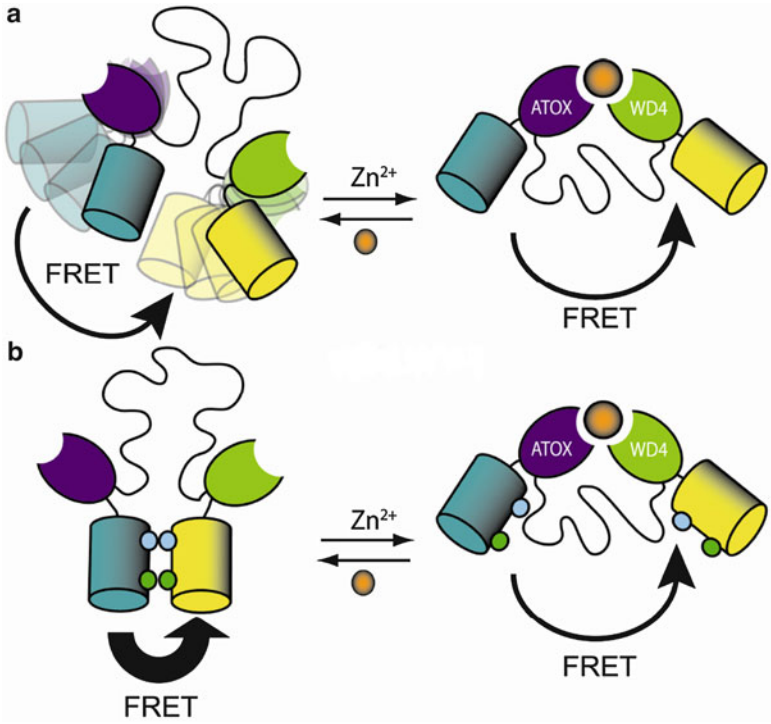

Fig. 7.1 Schematic representation of the CALWY (**a**) and eCALWY-1 (**b**) sensor designs, both consisting of two metal-binding domains, ATOX1 and WD4, connected via a flexible peptide linker and flanked by two fluorescent domains. **a** The CALWY sensor yielded a small Förster resonance energy transfer (FRET) change between the Zn^{2+}-free and Zn^{2+}-bound state. **b** In the eCALWY constructs two mutations, S208F and V224L, were introduced on both fluorescent domains, leading to high energy transfer in the Zn^{2+}-free state. Zn^{2+} binding disrupts the complex, resulting in a large decrease in FRET. (Adapted from Vinkenborg et al. 2009)

However, it was discovered that Zn^{2+} was able to form a very stable tetrahedral complex by binding the four cysteines present in the two copper-binding domains, yielding a K_d of approximately 0.23 pM at pH 7.1. Unfortunately, the change in emission ratio of the original CALWY sensor was small, showing a 15 % decrease in emission ratio upon Zn^{2+} binding. Because this poor dynamic would make the sensor less suitable for intracellular Zn^{2+} imaging, improved variants were developed, resulting in the so-called eCALWY series of Zn^{2+} sensors. First, ECFP and EYFP were replaced by cerulean and citrine, respectively, fluorescent domains with increased intensity (cerulean) and pH stability (citrine). Most importantly, the ratiometric response was improved sixfold by introduction of two mutations (S208F and V224L) on both cerulean and citrine that promote intramolecular complex formation between the two fluorescent domains in the absence of Zn^{2+}. Binding of Zn^{2+} to ATOX1 and WD4 disrupts the interaction between the fluorescent domains, resulting in a large decrease in FRET corresponding to a twofold

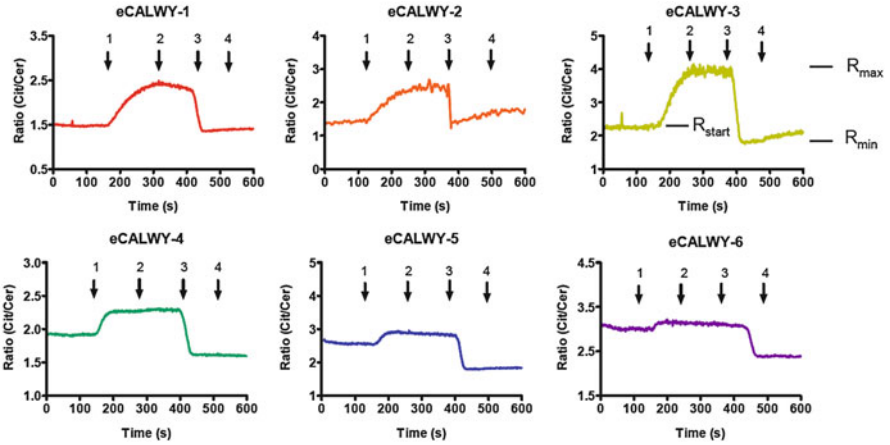

Fig. 7.2 Responses of single INS-1(832/13) cells expressing eCALWY-1–6 to addition of 50 μM TPEN (*1*), 5 μM pyrithione (*2*), 5 μM pyrithione/100 μM Zn^{2+} (*3*), and no additives (*4*). Traces show the responses of individual cells. In the response trace of eCALWY-3, the emission ratios used for R_{max}, R_{min}, and R_{start} are displayed. (Adapted from Vinkenborg et al. 2009)

change in emission ratio. As the interaction between the fluorescent domains competed with Zn^{2+} binding, the K_d for Zn^{2+} binding was attenuated by a factor of 10, resulting in a K_d of 2 pM at pH 7.1 (Fig. 7.1b) (Vinkenborg et al. 2009).

Without knowing the free cytosolic Zn^{2+} concentration in mammalian cells beforehand, eCALWY-1 was tested in HEK293 cells and INS-1(832/13) cells. Figure 7.2 shows the ratio of citrine to cerulean emission of a single cell using excitation of cerulean. Addition of the strong cell-permeable Zn^{2+} chelator TPEN results in an increase in emission ratio, consistent with dissociation of Zn^{2+} from the sensor. As expected, subsequent addition of the Zn^{2+} ionophore pyrithione and excess Zn^{2+} resulted in a decrease in emission ratio. This experiment showed that at the start of the experiment, the eCALWY-1 sensor was already fully occupied with Zn^{2+}, suggesting that the free cytosolic Zn^{2+} concentration was substantially higher than the 2 pM Zn^{2+} affinity of eCALWY-1. Therefore, a toolbox of eCALWY-based sensors was developed by systematically tuning the Zn^{2+} affinity of eCALWY-1. First, eCALWY-4 was created by introducing a single cysteine-to-serine mutation in the Zn^{2+}-binding pocket of the sensor, resulting in a 300-fold weakening of the affinity for Zn^{2+} ($K_d = 630$ pM) This mutation also abrogated Cu^{+} binding to the protein, as eCALWY-4 did not show any response up to micromolar Cu^{+} levels. Because the free cellular copper concentration has been estimated to be about 10^{-18} M (Wegner et al. 2010), Cu^{+} binding will not interfere with Zn^{2+} binding inside living cells. Further fine tuning of the Zn^{2+} affinity was achieved by shortening the flexible peptide linker between the metal-binding domains, yielding a series of Zn^{2+} sensors (eCALWY-1–6) with affinities ranging from low picomolar to low nanomolar and at least a twofold change in emission ratio upon Zn^{2+} binding at a physiological relevant pH (Table 7.1). Figure 7.2 shows the fluorescence

Table 7.1 Sensor properties of different Förster resonance energy transfer (FRET)-based Zn^{2+}

Sensor variant	Ratiometric change (in vitro)	K_d (pH 7.1)	Zn^{2+}-binding pocket
CALWY (Van Dongen et al. 2007)	15 %	0.2 pM	Cys_4
eCALWY-1 (Vinkenborg et al. 2009)	240 %	2 pM	Cys_4
eCALWY-2 (Vinkenborg et al. 2009)	270 %	9 pM	Cys_4
eCALWY-3 (Vinkenborg et al. 2009)	215 %	45 pM	Cys_4
eCALWY-4 (Vinkenborg et al. 2009)	250 %	630 pM	Cys_3
eCALWY-5 (Vinkenborg et al. 2009)	300 %	1,850 pM	Cys_3
eCALWY-6 (Vinkenborg et al. 2009)	200 %	2,900 pM	Cys_3
		0.5 μM (pH 6.0)	
redCALWY-1 (Lindenburg et al. 2013)	62 %	12.3 pM	Cys_4
redCALWY-4 (Lindenburg et al. 2013)	30 %	234 pM	Cys_3
ZifCY1 (Dittmer et al. 2009)	220 %	1.7 μM	Cys_2His_2
ZifCY2 (Dittmer et al. 2009)	400 %	160 μM	His_4
ZapCY1 (Qin et al. 2011)	130 %	2.5 pM	Cys_4
ZapCY2 (Qin et al. 2011)	70 %	811 pM	Cys_2His_2
ZapOC2 (Miranda et al. 2012)	12 % (in situ)	Nd	Cys_2His_2
ZinCh-9 (Evers et al. 2007)	360 %	213 nM (pH 8.0)	Cys_2
eZinCh-1 (Evers et al. 2007)	800 %	8.2 μM	Cys_2
		253 nM (pH 8.0)	
		250 μM (pH 6.0)	
CLY9-2His (Evers et al. 2008)	65 %	47 nM (pH 8.0)	2 His_6 tags

responses of INS-1(832/13) cells transiently expressing each of these six eCALWY variants upon addition of the membrane permeable Zn^{2+} chelator TPEN and subsequent treatment of Zn^{2+} and pyrithione. A consistent trend between sensor response and sensor affinity was observed, with the high-affinity eCALWY-1 being fully saturated whereas the sensor with the lowest affinity (eCALWY-6) was nearly empty at the start of the experiment.

For each of these sensors, the Zn^{2+} occupancy at the start of the experiment was calculated using Eq. (7.1). R_{max} and R_{min} are the steady-state ratios after TPEN and

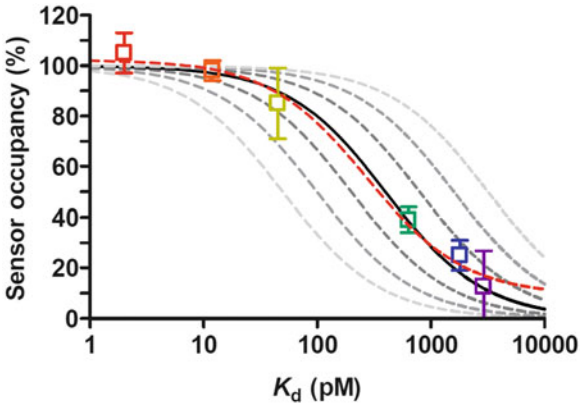

Fig. 7.3 Sensor occupancy in INS-1(832/13) cells as a function of the sensor K_d. Data points show the occupancy of the different eCALWY variants, determined from the traces of individual cells. A nonlinear least-squares fit yielded a free Zn^{2+} concentration of ~0.4 nM. The *dashed lines* depict the expected responses assuming free Zn^{2+} concentrations of 0.05, 0.1, 0.2, (0.4 *solid line*), 0.8, 1.6, and 3.2, respectively. (Adapted from Vinkenborg et al. 2009)

pyrithione/Zn^{2+} addition, respectively, and R_{start} is the ratio at the start of the experiment (Fig. 7.2).

$$\text{Occupancy} = \frac{R_{max} - R_{start}}{R_{max} - R_{min}} \cdot 100\ \% \tag{7.1}$$

Plotting the sensor occupancies for all six variants as a function of their K_d revealed that the sensor occupancies were consistent with a free Zn^{2+} concentration of about 0.4 nM (Fig. 7.3). The same results were obtained in mouse pancreatic beta cells (INS-1(832/13)) and in HEK293 cells. Although the cytosolic free Zn^{2+} concentration may also depend on cell type and conditions, subsequent work in other cell types and using these and other sensors (see following) has confirmed that the cytosolic Zn^{2+} in mammalian cells is relatively well-buffered between 100 pM and 1 nM. The observation that a single free Zn^{2+} concentration of 400 pM was sufficient to explain the occupancies of both high- and low-affinity sensors also indicates that the sensors do not significantly perturb the free Zn^{2+} concentration. In contrast to synthetic fluorescent Zn^{2+} sensors, which are added to the cells in relatively high concentrations at the time of the imaging experiment, genetically encoded fluorescent proteins are constitutively expressed and in this way become part of the cellular Zn^{2+} buffer machinery (Qin et al. 2013).

To gain further insight into the regulation of intracellular Zn^{2+} homeostasis and the possible role of Zn^{2+} as a secondary messenger, one would like to be able to monitor Zn^{2+} in different cellular compartments in the same cell at the same time or simultaneously monitor the relationship between Zn^{2+} concentration and other important signal transduction pathways such as Ca^{2+}, cAMP, and kinase activities. Therefore, spectrally distinct variants of the eCALWY sensors have recently been

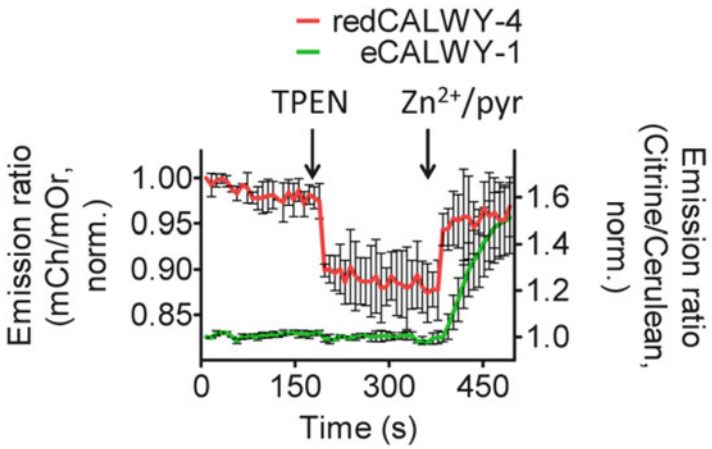

Fig. 7.4 Response of HeLa cells expressing both eCALWY-1 (*green*) and redCALWY-4 (*red*) to the addition of Zn^{2+}/pyrithione followed by excess TPEN. Traces represent the average of multiple cells after normalization of the emission ratio at $t = 0$. *Error bars* represent SEM. (Adapted from Lindenburg 2013)

developed that can be used together with CFP-YFP-based sensors (Lindenburg et al. 2013). These red fluorescent FRET sensors (redCALWYs) were obtained by replacing cerulean and citrine by mOrange and mCherry, respectively. Functional sensors were only obtained after reengineering the surface of both fluorescent domains to promote association of mOrange and mCherry in the Zn^{2+}-free state. Red versions were created of eCALWY-1 and eCALWY4.

In vitro characterization of redCALWY-1 and redCALWY-4 yielded K_d values of 12.3 ± 2 pM and 234 ± 5 pM, respectively (Table 7.1), which are comparable to the affinities of their CFP-YFP counterparts, showing that the replacement of the fluorescent domains had no effect on the ligand-binding properties. In situ characterization showed that the redCALWY-1 showed a response to addition of TPEN and Zn^{2+} similar to the original eCALWY-1 (Fig. 7.2), with both high-affinity sensors being completely saturated with Zn^{2+} under normal physiological conditions. Similarly, the lower-affinity redCALWY-4 was found to be mostly empty when expressed in the cytosol of HeLa cells. To explore the feasibility of using these redCALWY variants together with CFP-YFP-based systems, the high-affinity eCALWY-1 (CFP/YFP) was coexpressed with the lower-affinity redCALWY-4 in the cytosol of HeLa cells (Fig. 7.4). As expected, addition of Zn^{2+}/pyrithione to the cells resulted in a decrease in the redCALWY-4 emission ratio without affecting the eCALWY-1 emission ratio. Subsequent addition of TPEN resulted in a quick response for redCALWY-4, followed by a slower increase in emission ratio for the high-affinity eCALWY-1 sensor. In this case, simultaneous expression of spectrally distinct Zn^{2+} sensors with different affinities in the same cellular compartment increases the range over which the Zn^{2+} concentration can be monitored. More importantly, the experiment showed the feasibility of monitoring Zn^{2+}

concentrations at different subcellular localizations that otherwise cannot be easily distinguished, such as the ER and the cytosol.

In conclusion, the accurate determination of the cytosolic free Zn^{2+} concentration using the eCALWY sensors relies on several factors:

1. *The availability of sensors with a range of Zn^{2+} affinities*. Although the free Zn^{2+} concentration can be determined based on the occupancy of a single Zn^{2+} sensor and its in vitro determined K_d, such determinations are inherently less reliable than measurements based on sensors with different affinities, particularly when the sensor's affinity is not close to the free Zn^{2+} concentration. In the case of the eCALWY sensors, determination of the free Zn^{2+} concentration using eCALWY-4 is therefore more reliable than using for example eCALWY-2.
2. *Accurate determination of R_{max} and R_{min}*. The absolute emission ratio observed for cells expressing the same sensor may vary substantially between cells for example because of varying contributions of background fluorescence. Accurate determination of Zn^{2+} concentration therefore requires the determination of the emission ratio in the absence of Zn^{2+} (R_{max} in this case) and in the presence of Zn^{2+} (R_{min}). Accurate determination of R_{max} and R_{min} is helped in this case by the relatively fast association and dissociation kinetics of the sensor, allowing the establishments of stable plateau values within minutes following TPEN addition or even seconds after addition of Zn^{2+}/pyrithione.
3. *In situ calibration*. The calculation of the free Zn^{2+} concentration is based on the experimentally observed occupancies and the K_d of the sensor, which is most accurately determined in vitro. However, to rule out the possibility that the Zn^{2+} affinity is strongly affected by the intracellular conditions such as macromolecular crowding, ideally the sensor's affinity is also determined in situ. In situ calibration of eCALWY-4 using the pore-forming protein α-toxin and a Zn^{2+} buffer solution revealed that the in situ K_d was only slightly lower than that obtained in vitro using purified sensor protein.

7.2.2.2 Sensors Based on Zinc Fingers: Zif- and Zap-Based FRET Sensors

Because zinc fingers (ZFs) display metal-dependent protein folding and they typically show a high affinity and specificity for Zn^{2+}, they provide an attractive class of Zn^{2+}-binding domains for FRET sensor development. Although Zn^{2+} in most ZF domains plays solely a structural role, several examples of ZnF domains have also been reported that act as Zn^{2+}-dependent transcriptional regulators. The Palmer group has developed FRET sensors based on several different zinc-finger domains, providing access to FRET sensors with a range of affinities. The first series of FRET sensors was constructed using a ZF domain derived from the mammalian transcription factor Zif268, which contains a Cys_2His_2 binding motif (Dittmer et al. 2009). This well-characterized ZF is known to be largely unstructured in the absence of the metal ion and only folds upon Zn^{2+} binding. Two sensors were constructed by flanking the ZF domain with CFP and YFP, one containing the

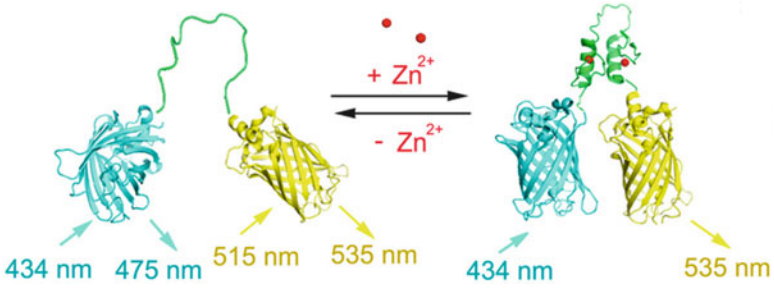

Fig. 7.5 Schematic representation of the high-affinity Zn^{2+} sensor ZapCY1, which consists of the first and second zinc finger of *Saccharomyces cerevisiae* Zap1 flanked by two fluorescent proteins, truncated CFP and citrine. (Adapted from Qin et al. 2013)

wild-type zinc-finger domain (ZifCY1) and a variant in which the cysteines in the original Cys2His2 motif were replace by two other histidines (ZifCY2). In vitro, a large increase in emission ratio was observed for both the ZifCY1 (2.2-fold) and the ZifCY2 (4-fold) sensors upon addition of Zn^{2+}. These in vitro Zn^{2+} titration experiments revealed Zn^{2+} affinities of 1.7 and ~160 μM for the ZifCY1 and ZifCY2 sensors, respectively. This affinity of the ZifCY1 sensor was surprisingly weak compared to the original Zif268 domain that contains a site with nanomolar affinity for Zn^{2+}. The origin of this large attenuation of Zn^{2+} affinity is not well understood but was attributed to the attachment of the fluorescent proteins. Both sensors were also tested by transiently expressing them in mammalian cell lines and monitoring their response to the addition of TPEN, followed by addition of digitonin (to permeabilize the cells) and subsequent Zn^{2+} addition. Unfortunately, the dynamic range of the ZifCY1 sensor was reduced to 25 %, possibly reflecting the effect of molecular crowding on decreasing the distance between the two fluorophores in the absence of zinc, resulting in an overall smaller ratiometric change. Despite the low Zn^{2+} affinity, the response of the ZifCY1 sensor was still used to estimate the cytosolic free Zn^{2+} concentration to be approximately 180 nM. This number merely reflected the lower limit of detection for this sensor, however, which also explained why higher sensor concentrations resulted in an apparent increase in the estimated intracellular Zn^{2+} level. This example illustrates the difficulty of measuring analyte concentrations that are outside the affinity range of a sensor, as the cytosolic Zn^{2+} concentration was subsequently shown to be 1,000 fold lower.

To overcome the low affinity and limited in situ dynamic range of the Zif268-based FRET sensors, Palmer and coworkers subsequently developed a series of FRET sensors based on zinc-finger domains from the yeast transcriptional regulator Zap1 (Qin et al. 2011). Instead of just a single ZF domain, these so-called Zap sensors consist of the first and second zinc fingers of *Saccharomyces cerevisiae* Zap1, which have low nanomolar affinity for Zn^{2+} (Fig. 7.5). FRET sensors based on these ZFs were actually first reported by Eide and coworkers (Qiao et al. 2006), who used them to learn more about the kinetics of Zn^{2+} binding and release to the

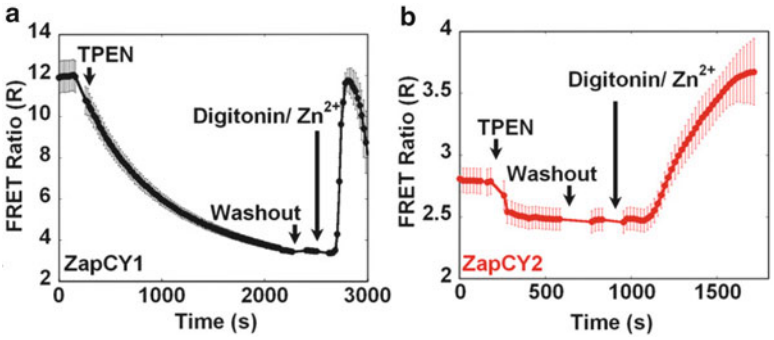

Fig. 7.6 FRET responses of ZapCY1 (**a**) and ZapCY2 (**b**) in the cytosol of HeLa cells ($n = 5$ cells). **a** ZapCY1 was fully saturated in the cytosol under resting conditions. **b** ZapCY2 was only partially saturated at the start of the experiment; free cytosolic Zn^{2+} concentration was estimated to be ~80 pM. (Adapted from Qin et al. 2011)

Zap1 zinc-finger domains. In the original study the sensors were not characterized in vitro and not used to measure the free Zn^{2+} concentration at the single-cell level. Palmer and coworkers improved these probes by introducing a truncated version of CFP and replacement of EYFP by the more pH stable citrine. To increase the dynamic range, the linker in the construct was also replaced by one previously used in genetically encoded Ca^{2+} sensors.

Determination of the Zn^{2+} affinity of the ZapCY1 sensor in vitro yielded a K_d of 2.5 pM at pH 7.4 (Fig. 7.6a). The Zn^{2+} affinity could be attenuated by replacing two of the cysteines in the zinc-finger domains by histidines again, yielding the ZapCY2 sensor, with a K_d of 811 pM. When ZapCY-1 was expressed in the cytosol of HeLa cells, a large fourfold decrease in emission ratio was observed upon treatment with a zinc-chelating reagent, which was completely reversed upon treatment of the cells with digitonin and excess Zn^{2+}. This response shows that the high-affinity ZapCY1 sensor was fully saturated under normal conditions. The lower-affinity ZapCY-2 sensor was only partially saturated in the cytosol under resting conditions (Fig. 7.6b), showed a 1.4-fold dynamic range, and could be used to estimate the free Zn^{2+} concentration in the cytosol to be ~80 pM, which is in the same range as determined using the eCALWY series.

A striking feature of the ZapCY-1 sensor is that prolonged incubations with TPEN are required to reach the Zn^{2+}-free state of the sensor. Part of this slow response may be an inherent feature of such high-affinity sensors, as the high-affinity eCALWY-1 sensor also showed a slower response than the intermediate-affinity eCALWY-4 sensor. Despite their similar affinities, the Zn^{2+}-free state of eCALWY-1 is reached within a few minutes, however, whereas this takes at least 30 min for ZapCY-1. The response of the lower-affinity ZapCY-2 to TPEN addition is much faster, making this the preferred Zap-based sensor for measuring cytosolic Zn^{2+} concentrations.

As for the eCALWY sensors, red-shifted variants have also been developed for the Zap-based FRET sensors. The CFP and YFP domains of the ZapCY1 and

ZapCY2 sensors were replaced by a variety of red-shifted donor and acceptor fluorescent domains, and sensor performance was tested for both cytosolic and nuclear-targeted sensors in HeLa cells, by doing an in situ calibration using TPEN and Zn^{2+}. Sensors with orange and red fluorescent domains, which are spectrally well separated from the CFP-YFP-based sensors, displayed relatively small changes in emission ratio of about 10 %. The highest in vivo dynamic range (40 %) was observed for sensors that used the green fluorescent protein Clover as donor and the red fluorescent protein mRuby2 as an acceptor. Using the latter sensors allowed the simultaneous measurement of Zn^{2+} concentration in different organelles, such as the nucleus and the cytosol, or the nucleus and the ER, Golgi, or mitochondria. The relatively modest dynamic range of the red-shifted sensor variants and the substantial spectral overlap between CFP/YFP- and Clover/mRuby2-based sensors precluded measurements in the same or overlapping intracellular compartments. The occupancies of the various sensors were sometimes found to be different, which suggests that replacing the fluorescent domains also affected Zn^{2+} affinity. Unfortunately, in vitro determination of the Zn^{2+} affinities of these new sensor variants was not reported.

7.2.2.3 eZinCh FRET Sensors and His-Tag-Based Sensors

The relatively high Zn^{2+} affinity of both the eCALWY and zinc-finger-based FRET sensors makes these the sensors of choice for imaging free cytosolic Zn^{2+} in mammalian cells. However, concentrations of free Zn^{2+} can differ substantially between cellular compartments, and the extracellular free Zn^{2+} concentration is known to be significantly higher. An example is provided by the insulin-secreting vesicles in pancreatic beta cells. The free Zn^{2+} concentrations in these vesicles was found to be high enough to completely saturate eCALWY-6, which at pH 6 binds Zn^{2+} with a K_d of 0.5 μM. Reliable measurements of these higher Zn^{2+} concentrations thus require the development of FRET sensors with sensitivities in the high nanomolar to micromolar region and sensors that cover a broader concentration range.

One example of these moderate-affinity sensors are the so-called ZinCh sensors (Evers et al. 2007). The ZinCh sensors do not contain separate Zn^{2+}-binding domains but consist of a fusion protein of ECFP and EYFP connected via a long flexible peptide linker of different lengths, in which two Zn^{2+}-coordinating amino acids (Y39H and S208C) were introduced at the dimer interface of both fluorescent domains (Fig. 7.7). A biphasic fourfold increase in emission ratio was observed upon addition of Zn^{2+}, corresponding to an increase in energy transfer efficiency from 50 % to 85 %. The first binding event ($K_d = 200$ nM at pH 8) involves the two Cys208 residues and results in formation of an intramolecular complex of ECFP and EYFP in a parallel orientation. After binding of Zn^{2+} to the high-affinity site, the two His39 are pre-organized to form a second, low-affinity Zn^{2+}-binding site ($K_{d2} \sim 88$ μM at pH 8.0), which results in a further increase in FRET. This sensor protein thus showed a large, fourfold increase in emission ratio over a broad range of Zn^{2+} concentrations between 100 nM and 1 mM. Importantly, ZinCh was shown

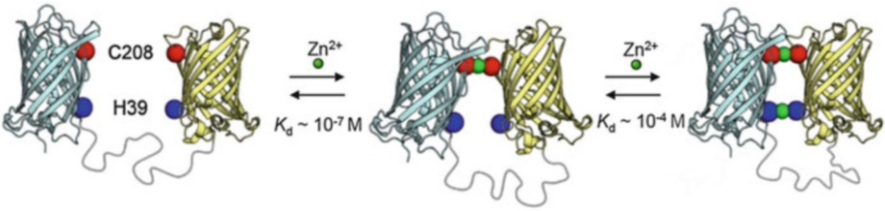

Fig. 7.7 Design of Zn^{2+}-chelating ECFP-EYFP chimera ZinCh-9. ECFP was fused to EYFP by a flexible $(GGSGGS)_9$ linker. A biphasic response was observed upon increasing Zn^{2+} concentrations, yielding a fourfold increase in emission ratio. (Adapted from Evers et al. 2007)

to be specific for Zn^{2+} over other divalent metal ions such as Cd^2, Ni^{2+}, Mg^2, and Ca^{2+}. More recently, the ECFP and EYFP domains were replaced by cerulean and citrine and the low-affinity site was deleted. This sensor, eZinCh-1, showed an even larger, eightfold increase in emission ratio and a similar Zn^{2+} affinity of $K_d = 258$ nM. The Zn^{2+} affinity of eZinCh-1 was also established under physiological relevant conditions, by determination of the Zn^{2+} affinity at pH 7.1 (cytosolic) and pH 6.0 (vesicular). Changing the pH from 8.0 to 7.1 resulted in a decrease in affinity to a K_d of 8.2 μM for Zn^{2+}, and K_d of ~250 μM at pH 6.0, most likely due to protonation of the cysteine residues ($pK_a = 8.3$) at lower pH. An initial effort to further increase the Zn^{2+} affinity of the eZinCh platform by introduction of additional flanking cysteine residues to create a tetrahedral Cys_4 site was not successful, as the Zn^{2+} affinities were in the same range as eZinch-1. This unimproved affinity suggests that only two of the four cysteines are involved in Zn^{2+} binding because the binding pocket is too large to tightly bind the Zn^{2+}. Indeed, Cd^{2+}, which has a larger ionic radius, was found to strongly bind to some of these Cys4 variants (Vinkenborg et al. 2011). Recently, our group found other eZinCh variants that display a substantially higher Zn^{2+} affinity, with a K_d of 1 nM at pH 7.1 and 200 nM at pH 6.0 (Hessels et al., unpublished results).

All the sensors discussed here rely at least partially on cysteines for Zn^{2+} binding, which renders these sensors redox sensitive and is the main reason for their pH sensitivity. Sensors based on histidine coordination are insensitive to oxidation and are predicted to be less sensitive to pH because of the lower pK_a of histidine. Based on the serendipitous discovery that Zn^{2+} forms a relatively stable 1:2 complex with His-tags, a FRET sensor was created by incorporating His-tags at the N- and C-termini of a fusion protein of ECFP and EYFP connected via a flexible peptide linker (Fig. 7.8). Addition of Zn^{2+} to this CLY9-2His sensor yielded a 1.6-fold increase in emission ratio, corresponding to a K_d of about 47 nM. The Zn^{2+} affinity of CLY9-2His is slightly higher than the afore-described ZinCh constructs. This sensor has not been used for intracellular imaging but has recently been applied to measure the free Zn^{2+} concentration in blood serum (Arts et al., unpublished results). This sensor variant may be improved further by replacing the ECFP and EYFP by cerulean and citrine and optimization of the linkers between the His-tags and the fluorescent domains. Such improved variants could be useful for intracellular imaging in oxidizing or acidic intracellular compartments.

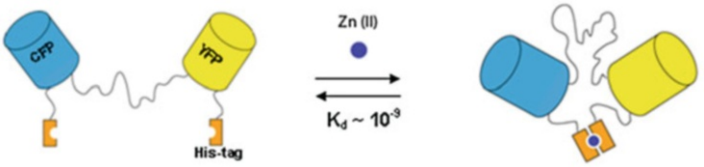

Fig. 7.8 Design of CLY9-2His containing both an N-terminal and a C-terminal His-tag. Zn^{2+} binding results in the formation of a compact intramolecular Zn^{2+} complex with a moderate Zn^{2+} affinity. (Adapted from Evers et al. 2008)

7.2.2.4 FRET Sensors Based on Binding of Fluorescently Labeled Sulfonamide to Carbonic Anhydrase

Thompson and coworkers have been developing fluorescent sensors based on carbonic anhydrase (CA), an enzyme with a single Zn^{2+}-binding site with picomolar affinity at pH 7.5 (Bozym et al. 2006). Carbonic anhydrase is one of the best studied enzymes, and a wealth of mutations are available that allow tuning of its Zn^{2+} affinity and Zn^{2+}-binding kinetics. In the original design, a FRET-based sensor was obtained by covalent attachment of Alexa Fluor 594 at a cysteine introduced at position 36, which acted as an acceptor for fluorescence from dapoxyl-sulfonamide, a fluorescent sulfonamide that binds strongly to the active site Zn^{2+}. The ratio of fluorescence observed at 617 nm obtained using dapoxyl excitation at 365 nm and direct AF594 excitation at 594 nm was used as a measure of the Zn^{2+} occupancy of the CA domain. To allow intracellular uptake of the fluorescently labeled CA, the probe was fused to a TAT peptide (Fig. 7.9).

Dissociation constants were obtained by determining calibration curves both on the microscope and a steady-state fluorometer, yielding $K_d \sim 70$ and ~137 pM, respectively. PC-12 cells were incubated with apoTAT-H36C-AF594-CA and dapoxyl-sulfonamide to measure free zinc levels inside the cell. A free Zn^{2+} concentration of 5 pM was obtained by direct comparison of the excitation ratio observed in the cell and the calibration curves. However, because no changes in emission ratio were observed upon addition of excess Zn^{2+} or strong Zn^{2+} chelators, in situ calibration of the sensor was not possible in this case, making the measurements more susceptible to variations in background fluorescence. Moreover, the performance of this system relies on the formation of a ternary complex between sensor, Zn^{2+}, and sulfonamide and thus assumes the presence of saturating concentrations of the latter of 1 μM. A fully genetically encoded version of the sensor protein was subsequently developed by fusing CA to dsRed2 as a FRET acceptor. This variant no longer requires protein transfection using the TAT peptide and could be targeted to the mitochondria of PC12 cells (McCranor et al. 2012). In situ calibration in isolated mitochondria revealed a K_d of 0.15 pM, which was substantially lower than the 17 pM determined for wtCA-dsRed2 in buffer and 70 pM determined for H36C-AF594-CA. Direct comparison of the excitation ratio yielded an apparent free Zn^{2+} concentration in the mitochondria of 0.15 pM.

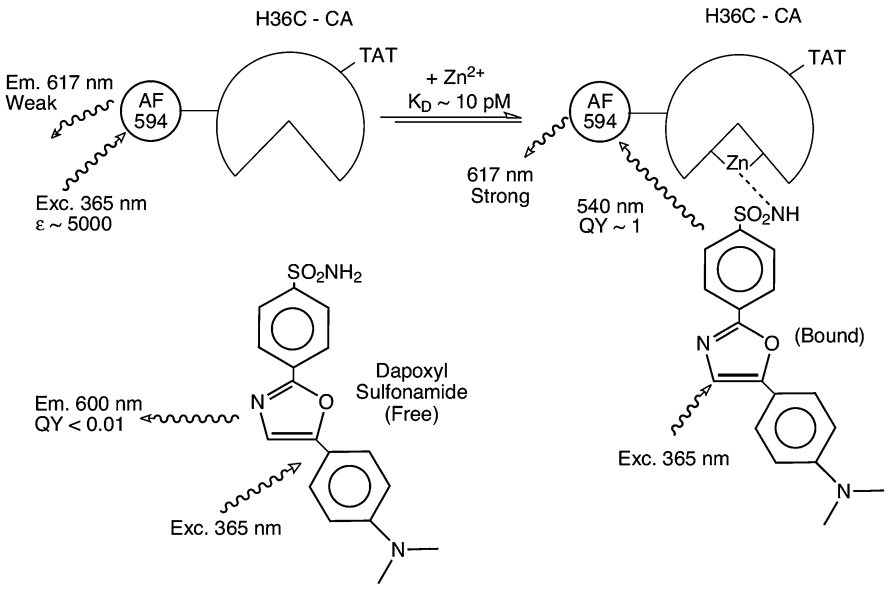

Fig. 7.9 Schematic representation of zinc ratiometric zinc determination with apoTAT-H36C-AlexaFluor 594 carbonic anhydrase and dapoxyl sulfonamide. In the absence of zinc, dapoxyl sulfonamide does not bind CA; therefore, no FRET occurs and very weak emission at 617 nm is observed. In the presence of zinc, dapoxyl sulfonamide binds to zinc, and FRET occurs from dapoxyl to the AlexaFluor 594. (Adapted from Bozym et al. 2006)

Both sensors just described are excitation ratiometric, which requires switching between two different lasers, and excitation of dapoxyl requires the use of 365-nm light, which may be damaging to the cells. Another sensor based on CA was therefore recently developed by the Thompson group (Zeng et al. 2013), in which the AF594 that is covalently attached to the CA acts as a donor. Chesapeake blue (CB) was coupled to the sulfonamide and can bind to the active protein in the presence of Zn^{2+}. In the absence of Zn^{2+}, the AF594 emits at 617 nm; when Zn^{2+} is bound to the protein, it promotes binding of the CB sulfonamide, resulting in emission at 650 nm. This red-shifted emission ratiometric sensor displayed a twofold change in emission ratio and bound Zn^{2+} with a $K_d \sim 5.8 \pm 3.1$ pM. The CB sulfonamide is highly charged, however, which prevents its application in intracellular imaging.

7.3 Applications of Genetically Encoded Sensors

In the previous section, the various types of genetically encoded fluorescent Zn^{2+} sensors were introduced and their in vitro and initial in situ characterization was described. In this section we discuss various subsequent applications such as their targeting to various subcellular compartments and their application in different cell types and organisms.

7.3.1 Subcellular Targeting of Genetically Encoded Sensors

One of the key distinguishing features of genetically encoded sensors is the relative ease by which they can be targeted to specific subcellular locations. Genetically encoded FRET sensors have been instrumental in establishing the concentration of free Zn^{2+} in a variety of cell types, revealing that cytosolic Zn^{2+} is well buffered between 0.1 and 1 nM. Successful determination of cytosolic Zn^{2+} concentrations critically depended on the availability of FRET sensors with the appropriate K_d and a robust calibration procedure to determine for each individual cell the emission ratio corresponding to Zn^{2+}-free and Zn^{2+}-bound state. In an effort to determine the free Zn^{2+} concentration in other organelles, several of the ZF-based FRET sensors developed in the Palmer laboratory were targeted to the ER, Golgi, and the mitochondrial matrix. Both the high-affinity ZapCY1 ($K_d \sim 2.5$ pM) and the low-affinity ZifCY1 ($K_d \sim 1.7$ μM) sensor were targeted to the lumen of the ER and the inner surface of the Golgi membrane (Qin et al. 2011). The targeting was confirmed by colocalization using commercially available markers to the desired organelles. HeLa cells expressing ER-ZapCY1 showed a slow and small decrease in emission ratio following addition of TPEN (Fig. 7.10a), followed by a much larger increase in emission ratio upon addition of excess Zn^{2+}. For cells expressing the low-affinity ER-ZifCY1 (Fig. 7.10b), no decrease in FRET was observed upon TPEN addition, suggesting that the free Zn^{2+} level in the ER was below the detection limit of this sensor. Equation 7.1 was used to calculate the free Zn^{2+} concentration in the ER under resting conditions by using R_{min} and R_{max} for calibration, yielding a free Zn^{2+} in the ER of 0.9 pM. The same experiments were performed in the Golgi (Fig. 7.10c, d), yielding a similarly low free Zn^{2+} of 0.6 pM.

These data would suggest that the free Zn^{2+} concentration in the ER and Golgi of mammalian cells is maintained at an even lower concentration than is present in the cytosol. One potential caveat of these measurements is the slow rate of Zn^{2+} release from the sensor upon TPEN addition, which makes it more difficult to accurately determine R_{min}. Very different results were recently obtained by the Rutter and Merkx groups, who used ER-targeted eCALWY-4 to probe the Zn^{2+} concentration in the ER. This probe, which has an affinity of 600 pM, was found to be mostly saturated with Zn^{2+} in a variety of cell lines and primary cardiomyocytes (Chabosseau et al. 2014). These results would suggest that the free Zn^{2+} concentration in the ER is at least 5 nM, which would be consistent with recent suggestions that the ER acts as a store for Zn^{2+} (Taylor et al. 2012). Taylor and coworkers recently proposed a model whereby phosphorylation of ZIP7 plays a role in release of Zn^{2+} from ER stores into the cytosol.

FRET sensors have also been targeted to the mitochondrial matrix. Palmer and coworkers appended an N-terminal mitochondrial targeting sequence from human cytochrome *c* oxidase subunit 8a to both Zif- and Zap-based FRET sensors, yielding

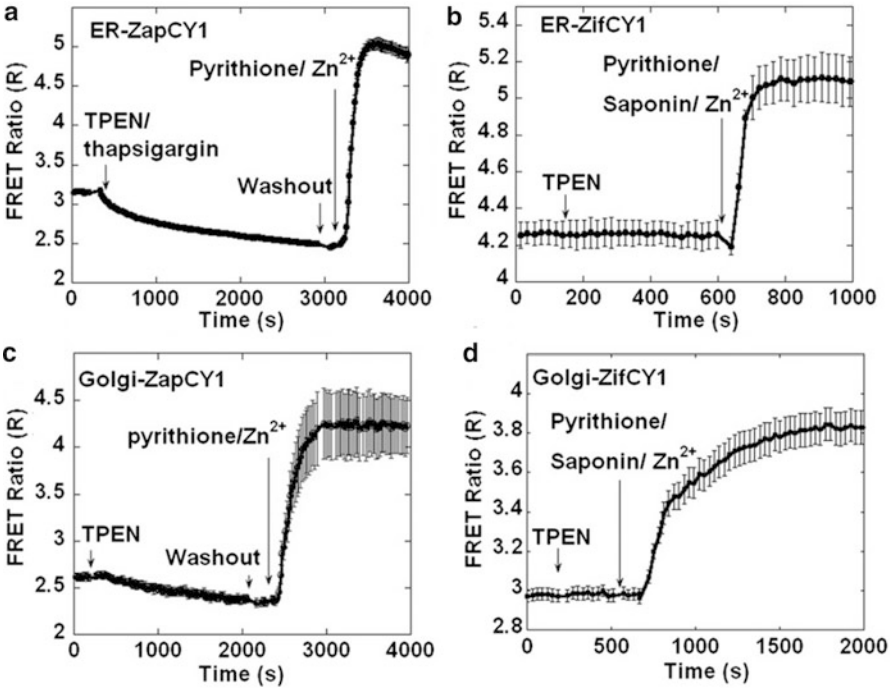

Fig. 7.10 Representative traces for ER-ZapCY1 (**a**) and ER-ZifCY1 (**b**). **a** The FRET ratio decreased upon addition of 150 μM TPEN/10 μM thapsigargin and increased with addition of 5 μM pyrithione and 10 nM Zn^{2+}. **b** No change in FRET ratio was observed upon TPEN addition, but addition of 25 μM pyrithione/saponin/500 μM Zn^{2+} resulted in an increase in emission ratio. Representative traces for Golgi-ZapCY1 (**c**) and Golgi-ZifCY1 (**d**). **c** The FRET ratio decreased upon addition of 150 μM TPEN and increased with addition of 5 μM pyrithione and 10 nM Zn^{2+}. **d** No change in FRET ratio was observed upon TPEN addition, but addition of 25 μM pyrithione/saponin/500 μM Zn^{2+} resulted in an increase in emission ratio. (Adapted from Qin et al. 2011)

mito-ZapCY1 and mito-ZifCY1. Colocalization studies using MitoTracker Red confirmed excellent targeting. Based on measurements with the low-affinity mito-ZifCY1, the mitochondrial free Zn^{2+} concentration was initially reported to be 680 nM. However, this number was found to be unreliable because of the poor dynamic range of mito-ZifCY1 as new variants with a larger dynamic range were found to be essentially unsaturated (Park et al. 2012; Dittmer et al. 2009). Targeting of the high-affinity ZapCY1 sensor to the mitochondria showed a response to TPEN and Zn^{2+}/pyrithione addition that is very similar to that of ER- and Golgi-targeted Zap-CY1; that is, addition of TPEN induces a small decrease in emission ratio over a period of an hour, whereas subsequent addition of excess Zn^{2+} results in a much larger and rapid increase in emission ratio. Based on this response and correcting for the even higher affinity of ZapCY1 at the mitochondrial pH of 8, the free mitochondrial Zn^{2+} concentration was estimated to be 0.22 pM in HeLa cells.

Somewhat higher sensor occupancies of 50 % were observed in MIN6 and primary neurons. These surprisingly low concentrations are 300 fold lower than what was recently determined using a small-molecule Zn^{2+} fluorescent sensor (Xue et al. 2012) that contained a triphenylphosphonium (TPP) group as an effective mitochondrial targeting ligand. The K_d of this probe was determined to be about 150 pM at mitochondrial pH and a free mitochondrial Zn^{2+} concentration of about 72 pM was measured in NIH 3T3 cells. Recent measurements of mitochondrial Zn^{2+} using the eCALW-4 sensor targeted to the mitochondrial matrix consistently yielded free Zn^{2+} concentrations of 200–300 pM in a number of cell lines and primary cells (Chabosseau et al. 2014). Thus, the ER and mitochondrial zinc concentrations determined using the eCALWY probes are three orders of magnitude higher than calculated using the targeted ZapCY1 probes (Park et al. 2012; Qin et al. 2011). This discrepancy is likely not the result of an error in determining the Zn^{2+} affinities of one of the sensors, as the eCALWY sensors and ZapCY1/CY2 sensors give much more consistent results when applied in the cytosol. A striking feature of the ZapCY1 sensor is its slow dissociation kinetics, which required more than 1 h incubation in TPEN to achieve the fully Zn^{2+}-depleted state,(Qin et al. 2011) compared to 2–3 min for the equivalent eCALWY probe (Fig. 7.2). In general, rapid equilibration makes the determination of $R_{0\%}$ and $R_{100\%}$ less sensitive to baseline drift, and prolonged incubations with TPEN have also been reported to be cytotoxic (Hashemi et al. 2007; Donadelli et al. 2008) Nonetheless, why the eCALWY- and ZapCY-based sensors behave so differently when targeted to the ER and mitochondria remains to be explained. One way to resolve these discrepancies might be to use FRET sensors that have alternative binding mechanisms. The current sensors depend on cysteines for Zn^{2+} coordination, which may result in formation of disulfide bonds or misfolding in the oxidizing environment of the ER lumen.

Secretory vesicles in many cell types contain highly elevated Zn^{2+} concentrations including those involved in neurotransmission, the prostate, and the insulin-containing vesicles of pancreatic β cells. The only example of a genetically encoded sensor targeting a secretory vesicle has been reported by Vinkenborg et al. Both the high-affinity sensors eCALWY-1 and eCALWY-6 and the low-affinity eZinCh-1 sensor were targeted to the secretory granules of INS-1(832/13) cells by fusion to vesicle-associated membrane protein 2 (VAMP2). Zn^{2+} is known to be important for insulin storage and secretion, and stable insulin Zn^{2+} complexes are formed in the acidic (pH 6.0) interior of these vesicles. Mutations in Znt8, a Zn^{2+}-specific importer protein that is exclusively localized in the secretory granules, have also been linked to the development of diabetes (Murgia et al. 2009). Colocalization studies of these vesicular-targeted constructs showed exclusive localization in insulin-containing granules (Fig. 7.11a). Emission ratios of the cells expressing either one of the sensors were monitored; for the eCALWY variants, low emission ratios were observed, indicating that the sensors were already fully saturated with Zn^{2+} at the start of the experiment. On the other hand, the low affinity eZinCh-1 appeared to be empty at this stage. None of the sensors showed changes in emission ratio upon addition of either TPEN or Zn^{2+}/pyrithione, suggesting that at high free

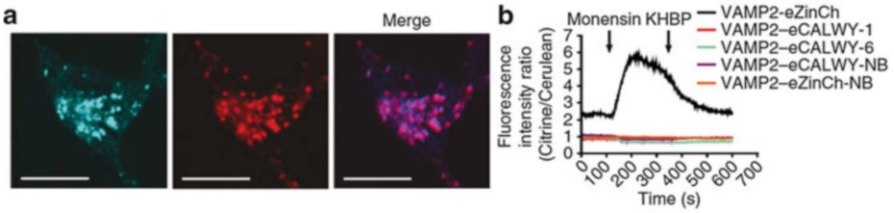

Fig. 7.11 Subcellular targeting of Zn^{2+} probes to insulin-storing vesicles. **a** Confocal laser microscopy images of INS-1(832/13) cells transfected with plasmids encoding VAMP2-eCALWY-1 (*left*) and neuropeptide Y-mCherry (*middle*). **b** Ratiometric response of INS-1 (832/13) cells expressing different VAMP2 constructs to 10 μM monensin (*1*), followed by buffer without compounds (*2*). (Adapted from Vinkenborg et al. 2009)

Zn^{2+} concentrations TPEN is unable to remove the Zn^{2+} from the high-affinity eCALWY variants ($K_d = 0.5$ μM at pH 6.0 for eCALWY-6). At the same time, it is probably also difficult to raise the free Zn^{2+} concentration inside the vesicles to the millimolar (mM) concentrations that are required to saturate the low-affinity eZinCh-1 sensor (K_d 250 μM at pH 6.0; Table 7.1). To test the hypothesis that eZinCh-1 was indeed nearly empty because of the low vesicular pH, cells were treated with the Na^+/H^+ exchanger monensin, which transiently increases the pH from 6 to 7. As expected, a reversible increase in emission ratio was observed for cells expressing VAMP2-eZinCh-1 as a result of simultaneous Zn^{2+} release from the insulin-Zn^{2+} and increase in affinity of eZinCh-1 (Fig. 7.11b). Although this experiment established the functionality of vesicular-targeted eZinCh-1, it also showed that accurate determination of (fluctuations in) vesicular free Zn^{2+} concentrations requires the development of less pH sensitive FRET sensors with a Zn^{2+} affinity of about 10 μM at pH 6.0.

7.3.2 Applications in Primary Cells and Plants

Genetically encoded fluorescent Zn^{2+} sensors have been mostly used in cell lines using transient transfection. To study Zn^{2+} homeostasis in primary pancreatic β cells, Rutter and coworkers cloned several eCALWY-variants into a pShuttle vector to allow transfection of primary cells using adenovirus (Bellomo et al. 2011). pShuttle-eCALWY constructs were digested with Pme1 and electroporated into competent BJ5183-AD-1 cells. Recombined pADeasy1 clones were screened, and positive clones were then digested with Pac1 and transfected into HEK293 cells for the generation of adenoviral particles. Primary islet cells were infected with eCALWY-4-expressing adenovirus and used to measure free cytosolic Zn^{2+}. High glucose concentrations were found to induce an increase in the cytosolic free Zn^{2+} concentration. Cytosolic free Zn^{2+} concentrations were found to be twofold higher in cells 24 h after being treated with high glucose concentrations (16.7 mM) compared to cells treated with low (3 mM) glucose concentrations,

853 pM Zn^{2+} versus 452 pM Zn^{2+}, respectively. These findings are in contrast with the work done by Zalewski et al., who observed a decrease in cytosolic Zn^{2+} in islet cells in response to glucose (Zalewski et al. 1994). They used a synthetic probe (Zinquin) to perform their measurements, however, which partly localizes in granules and other membrane-bound organelles where the free Zn^{2+} concentration is higher than in the cytosol. Therefore, the observed free Zn^{2+} concentrations and changes may be caused by degranulation of cells in response to glucose. Other primary cells in which FRET sensors have been used include primary neurons (Park et al. 2012) and cardiomyocytes (Chabosseau et al. 2014).

Several techniques have been used to investigate cellular distribution of total Zn^{2+} in plants, but until recently genetically encoded sensors have not been used in plants (Lanquar et al. 2005). The chemical probe Zinpyr-1 was used to study the role of Zn^{2+} in plants (Sinclair et al. 2007), but several issues were apparent, including problems with cellular penetration, control over intracellular localization, and long-term imaging possibilities. The Frommer group therefore recently constructed transgenic *Arabidopsis thaliana* lines that each constitutively express different cytosolic eCALWY variants (Lanquar et al. 2014). Low or no fluorescence was observed in the Col-O ecotype, indicating transgene-induced silencing. Therefore, the eCALWY variants were also expressed in the rgr6 line, which is deficient in transgene-induced silencing. Transgenic plant lines showing high and homogeneous fluorescence in this genetic background were selected. These eCALWY-expressing *Arabidopsis* lines looked normal and healthy and did not show a change in bulk Zn concentration. To avoid background fluorescence and easy imaging, Zn^{2+} homeostasis was imaged in root cells using the so-called RootChip setup. To determine the cytosolic Zn^{2+} concentration, the sensor occupancy was measured for each sensor as a function of the K_d of the sensor. For the plants grown in the presence of normal concentrations of Zn^{2+} (5 μM), the free cytosolic Zn^{2+} concentration was determined to be about 420 pM, the same value was found in mammalian cells using the same FRET sensors (Fig. 7.12). A concentration of about 2 nM was found for plants grown at excess Zn^{2+}, and the estimated free cytosolic Zn^{2+} concentration in starved root cells was about 1.5 nM, although a high standard error was observed under Zn^{2+}-depleted conditions. Monitoring the dynamic response of cytosolic Zn^{2+} to external supply suggested the involvement of high- and low-affinity uptake systems as well as release from internal stores.

7.4 Conclusion

Genetically encoded Zn^{2+} sensors have proven themselves as a valuable alternative to the use of synthetic fluorescent dyes for monitoring intracellular Zn^{2+} homeostasis and signaling. FRET-based fluorescent sensor proteins are attractive because they do not require cell-invasive procedures, they allow ratiometric detection, their concentration can be tightly controlled, and they can be targeted to different locations in the cell. FRET-based sensors developed by our group and others

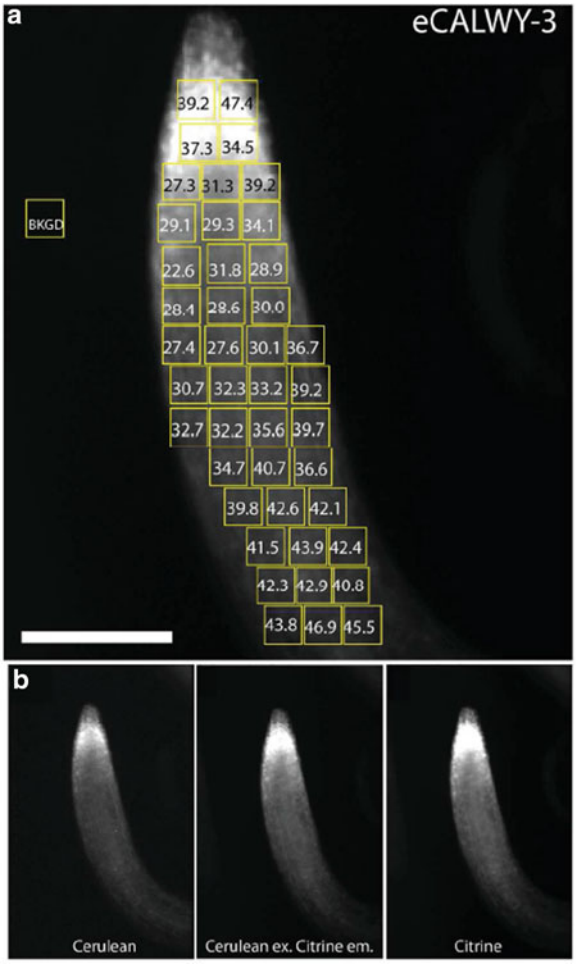

Fig. 7.12 Images displaying the expression of eCALWY-3 in *Arabidopsis thaliana* roots. **a** The numbers reflect sensor occupancy values calculated for each region of interest. **b** Expression pattern of the sensor in each channel for the same root: cerulean emission (*left*), citrine emission upon cerulean excitation (*middle*), and citrine emission (*right*). (Adapted from Lanquar et al. 2014)

have been instrumental to establish that the cytosolic levels of free zinc in mammalian cells are tightly regulated at around 0.5 nM. An important recent addition to the toolbox of sensors is the development of red-shifted variants, which permits the simultaneous imaging of Zn^{2+} in different cellular compartments such as the ER and the cytosol, but also provides an opportunity to study the spatiotemporal relationship between Zn^{2+} signaling and other intracellular signaling pathways. Targeting of FRET sensors to organelles has revealed conflicting results, with one sensor type (ZapCY-1) reporting extremely low levels of free Zn^{2+} in the ER, Golgi, and mitochondria, whereas much higher levels (>1,000 fold) have been observed for the eCALWY system when targeted to the ER and mitochondria in different cell lines and primary cells. These conflicting results may be resolved by the development of new FRET sensors based on different binding mechanisms. Other items on the to-do list include the development of probes that are redox

insensitive, less pH sensitive, and have affinities tuned to specific applications, such as measuring Zn^{2+} in secretory vesicles, extracellular Zn^{2+} in the brain, and Zn^{2+} in blood plasma. Their genetic encoding should allow easy distribution of these probes throughout the research community and the generation of transgenic organisms to study Zn^{2+} homeostasis and signaling in a variety of model organisms.

Acknowledgments The work of the authors on genetically encoded fluorescent probes is supported by grants from The Netherlands Organization of Scientific Research (VIDI grant 700.56.428 and ECHO grant 700.59.013) and an ERC starting grant (ERC-2011-StG 280255).

References

Barondeau DP, Kassmann CJ, Tainer JA, Getzoff ED (2002) Structural chemistry of a green fluorescent protein Zn biosensor. J Am Chem Soc 124:3522–3524

Bellomo EA, Meur G, Rutter GA (2011) Glucose regulates free cytosolic Zn^{2+} concentration, Slc39 (Zip), and metallothionein gene expression in primary pancreatic islet beta-cells. J Biol Chem 286:25778–25789

Bozym RA, Thompson RB, Stoddard AK, Fierke CA (2006) Measuring picomolar intracellular exchangeable zinc in Pc-12 cells using a ratiometric fluorescence biosensor. ACS Chem Biol 1:103–111

Chabosseau P, Tuncay E, Meur G, Bellomo EA, Hessels, AM, Hughes S, Johnson PRV, Bugliani M, Marchetti P, Turan B, Lyon AR, Merkx M, Rutter GA (2014) ACS Chem Biol in press (doi:10.1021/cb5004064)

Cousins RJ, Liuzzi JP, Lichten LA (2006) Mammalian zinc transport, trafficking, and signals. J Biol Chem 281:24085–24089

Dittmer PJ, Miranda JG, Gorski JA, Palmer AE (2009) Genetically encoded sensors to elucidate spatial distribution of cellular zinc. J Biol Chem 284:16289–16297

Domaille DW, Que EL, Chang CJ (2008) Synthetic fluorescent sensors for studying the cell biology of metals. Nat Chem Biol 4:168–175

Donadelli M, Dalla Pozza E, Costanzo C, Scupoli MT, Scarpa A, Palmieri M (2008) Zinc depletion efficiently inhibits pancreatic cancer cell growth by increasing the ratio of antiproliferative/proliferative genes. J Cell Biochem 104:202–212

Evers TH, Appelhof MA, De Graaf-Heuvelmans PT, Meijer EW, Merkx M (2007) Ratiometric detection of Zn(II) using chelating fluorescent protein chimeras. J Mol Biol 374:411–425

Evers TH, Appelhof MA, Meijer EW, Merkx M (2008) His-tags as Zn(II) binding motifs in a protein-based fluorescent sensor. Protein Eng Des Sel 21:529–536

Hashemi M, Ghavami S, Eshraghi M, Booy EP, Los M (2007) Cytotoxic effects of intra and extracellular zinc chelation on human breast cancer cells. Eur J Pharmacol 557:9–19

Ho LH, Riuffin RE, Murgia C, Li XL, Krilis SA, Zalewski PD (2004) Labile zinc and zinc transporter Znt4 in mast cell granules: role in regulation Nf-Kb translocation. J Immunol 172:7750–7760

Hutton JC, Penn EJ, Peshavaria M (1983) Low-molecular weight constituents of isolated insuline-secretory granules: bivalent-cations, adenine-nucleotides and inorganic phosphates. Biochem J 210:297–305

Kikuchi K (2010) Design, synthesis and biological application of chemical probes for bio-imaging. Chem Soc Rev 39:2048–2053

Krezel A, Maret W (2006) Zinc-buffering capacity of a eukaryotic cell at physiological P_{zn}. J Biol Inorg Chem 11:1049–1062

Lanquar V, Lelievre F, Bolte S, Hames C, Alcon C, Neumann D, Vansuyt G, Curie C, Schroder A, Kramer U, Barbier-Brygoo H, Thomine S (2005) Mobilization of vacuolar iron by Atnramp3 and Atnramp4 is essential for seed germination on low iron. EMBO J 24:4041–4051

Lanquar V, Grossmann G, Vinkenborg JL, Merkx M, Thomine S, Frommer WB (2014) Dynamic imaging of cytosolic zinc in *Arabidopsis* roots combining fret sensors and rootchip technology. New Phytol 202:198–208

Lindenburg LH, Hessels AM, Ebberink EH, Arts R, Merkx M (2013) Robust red FRET sensors using self-associating fluorescent domains. ACS Chem Biol 8:2133–2139

Linkous DH, Flinn JM, Koh JY, Lanzirotti A, Bertsch PM, Jones BF, Giblin LJ, Frederickson CJ (2008) Evidence that the Znt3 protein controls the total amount of elemental zinc in synaptic vesicles. J Histochem Cytochem 56:3–6

Liu J, Karpus J, Wegner SV, Chen PR, He C (2013a) Genetically encoded copper(I) reporters with improved response for use in imaging. J Am Chem Soc 135:3144–3149

Liu X, Li J, Hu C, Zhou Q, Zhang W, Hu M, Zhou J, Wang J (2013b) Significant expansion of the fluorescent protein chromophore through the genetic incorporation of a metal-chelating unnatural amino acid. Angew Chem Int Ed Engl 52:4805–4809

McCranor BJ, Bozym RA, Vitolo MI, Fierke CA, Bambrick L, Polster BM, Fiskum G, Thompson RB (2012) Quantitative imaging of mitochondrial and cytosolic free zinc levels in an in vitro model of ischemia/reperfusion. J Bioenerg Biomembr 44:253–263

Miranda JG, Weaver AL, Qin Y, Park JG, Stoddard CI, Lin MZ, Palmer AE (2012) New alternately colored fret sensors for simultaneous monitoring of Zn^{2+} in multiple cellular locations. PLoS One 7:E49371

Mizuno T, Murao K, Tanabe Y, Oda M, Tanaka T (2007) Metal-ion-dependent GFP emission in vivo by combining a circularly permutated green fluorescent protein with an engineered metal-ion-binding coiled-coil. J Am Chem Soc 129:11378–11383

Murgia C, Devirgiliis C, Mancini E, Donadel G, Zalewski P, Perozzi G (2009) Diabetes-linked zinc transporter Znt8 is a homodimeric protein expressed by distinct rodent endocrine cell types in the pancreas and other glands. Nutr Metab Cardiovasc Dis 19:431–439

Nolan EM, Lippard SJ (2009) Small-molecule fluorescent sensors for investigating zinc metalloneurochemistry. Acc Chem Res 42:193–203

Park JG, Qin Y, Galati DF, Palmer AE (2012) New sensors for quantitative measurement of mitochondrial Zn^{2+}. ACS Chem Biol 7:1636–1640

Qiao W, Mooney M, Bird AJ, Winge DR, Eide DJ (2006) Zinc binding to a regulatory zinc-sensing domain monitored in vivo by using fret. Proc Natl Acad Sci USA 103:8674–8679

Qin Y, Dittmer PJ, Park JG, Jansen KB, Palmer AE (2011) Measuring steady-state and dynamic endoplasmic reticulum and Golgi Zn^{2+} with genetically encoded sensors. Proc Natl Acad Sci USA 108:7351–7356

Qin Y, Miranda JG, Stoddard CI, Dean KM, Galati DF, Palmer AE (2013) Direct comparison of a genetically encoded sensor and small molecule indicator: implications for quantification of cytosolic Zn^{2+}. ACS Chem Biol 8:2366–2371

Rae TD, Schmidt PJ, Pufahl RA, Culotta VC, O'Halloran TV (1999) Undetectable intracellular free copper: the requirement of a copper chaperone for superoxide dismutase. Science 284:805–808

Sinclair SA, Sherson SM, Jarvis R, Camakaris J, Cobbett CS (2007) The use of the zinc-fluorophore, zinpyr-1, in the study of zinc homeostasis in *Arabidopsis* roots. New Phytol 174:39–45

Taylor KM, Hiscox S, Nicholson RI, Hogstrand C, Kille P (2012) Protein kinase Ck2 triggers cytosolic zinc signaling pathways by phosphorylation of zinc channel Zip7. Sci Signal 5:ra11

Valko M, Morris H, Cronin MT (2005) Metals, toxicity and oxidative stress. Curr Med Chem 12:1161–1208

Van Dongen EM, Dekkers LM, Spijker K, Meijer EW, Klomp LW, Merkx M (2006) Ratiometric fluorescent sensor proteins with subnanomolar affinity for Zn(II) based on copper chaperone domains. J Am Chem Soc 128:10754–10762

Van Dongen EMWM, Evers TH, Dekkers LM, Meijer EW, Klomp LWJ, Merkx M (2007) Variation of linker length in ratiometric fluorescent sensor proteins allows rational tuning of Zn(II) affinity in the picomolar to femtomolar range. J Am Chem Soc 129:3494–3495

Vinkenborg JL, Nicolson TJ, Bellomo EA, Koay MS, Rutter GA, Merkx M (2009) Genetically encoded fret sensors to monitor intracellular Zn^{2+} homeostasis. Nat Methods 6:737–740

Vinkenborg JL, Van Duijnhoven SM, Merkx M (2011) Reengineering of a fluorescent zinc sensor protein yields the first genetically encoded cadmium probe. Chem Commun (Camb) 47:11879–11881

Wegner SV, Arslan H, Sunbul M, Yin J, He C (2010) Dynamic copper(I) imaging in mammalian cells with a genetically encoded fluorescent copper(I) sensor. J Am Chem Soc 132:2567–2569

Xue L, Li G, Yu C, Jiang H (2012) A ratiometric and targetable fluorescent sensor for quantification of mitochondrial zinc ions. Chemistry 18:1050–1054

Zalewski PD, Millard SH, Forbes IJ, Kapaniris O, Slavotinek A, Betts WH, Ward AD, Lincoln SF, Mahadevan I (1994) Video image analysis of labile zinc in viable pancreatic islet cells using a specific fluorescent probe for zinc. J Histochem Cytochem 42:877–884

Zeng HH, Matveeva EG, Stoddard AK, Fierke CA, Thompson RB (2013) Long wavelength fluorescence ratiometric zinc biosensor. J Fluoresc 23:375–379